Paradigm Shift in the Indication of a Stable Cell during Power Modulation

Roman Düssel
Reduction Manager
TRIMET Aluminium SE, Essen, Germany
Roman.Duessel@trimet.de

Abstract

A megatrend of the next decades is the energy transition from conventional power to renewable. Adapting the aluminium smelting process to a flexible power supply needs the rethinking of a number of aspects in the smelting process. Manipulating thermal and magnetic impacts associated with amperage changes are just a few of these aspects.

The core element of our Virtual Battery is our newly developed control system. Conventional pot control systems are designed for conventional operations and static process targets. This becomes obsolete or even contradictory when operating with power modulation. Hence we need a different approach.

The approach that is outlined here is divided into three areas. The first step is to reduce the energy input as far as possible and to compensate in a subsequent step the heat loss by heat exchangers. Each cell is subject to thermal and process engineering limits, which were intended for the cell at TRIMET Essen. If the minimum cell resistance and the min/max limits of the heat losses are well known, the regulation of the heat balance can be done by changing the resistance. According to Ohm's law the resistance can be adjusted to its minimum inversely proportionally to the current. After reaching the resistance minimum, the heat loss through the heat exchanger is increased in proportion to further current increases. Finally control systems of an existing process control must be adjusted so that it does not counteract the energy flexibility, but promote it. The limits and values, such as temperatures and their deviations, of operating a cell have to be modified and the meaning of a stable cell rethought.

Keywords: Aluminium reduction cell process control, virtual battery, energy demand management, renewable energy, real-time heat balance control, energy counter.

1. History of Power Modulation

The idea of current modulation using aluminum electrolysis cells is not new; as early as in the 1990s, experiments were carried out in electrolysis cells in Brazil [1, 2]. Load management was also already an issue in 1974 in the electrolysis in Essen. Alusuisse engineers [3, 4] made various calculations for power reduction. Their ideas, however, mainly involved turning off pots rather than modulating them with the help of amperage. The innovation of load management nowadays is that over a certain period of time production volume and thus performance are kept constant. The modulation takes place for only a short time and above all with a faster change. This development was accelerated by the addition of renewable energies to the grid and therefore changed the time of the generation of electricity tremendously. Figure 1 shows the production and consumption profile predicted for the year 2050, showing the deficit in red and the surplus in green.

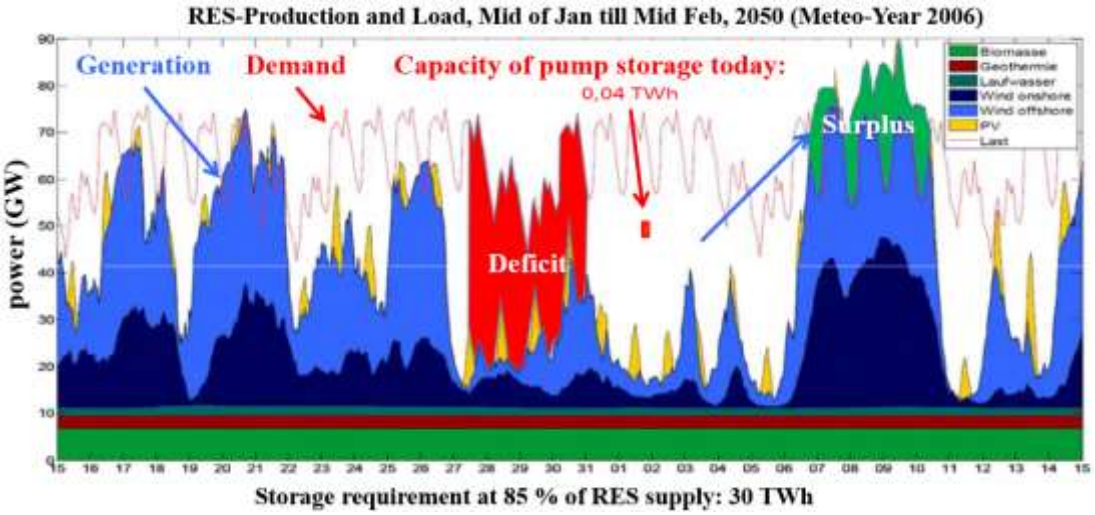

Figure 1. Production and consumption profile for the year 2050 [5].

The novel mode of modulation has negative effects on the process efficiency, which is designed for a stable energy balance. The essential point is to find out when the efficiency drops sharply and to optimize the process to further delay this point in time. The core of the new mode of production is to interpret the old philosophy correctly. The cell needs a consistent energy balance and not a constant energy input. Ultimately, economic consideration is once again a decision maker between gaining modulation revenue and losing process efficiency.

2. Theory of Side Ledge Changes

The change of the heat loss during the modulation over the period t corresponds to the changed enthalpy of the cell. This can be stated at time t as follows [6]:

$$\Delta\dot{Q}_I = mc_p \frac{dT}{dt} \tag{1}$$

where:

$\Delta\dot{Q}_I$	Heat flow rate, W
m	Mass, kg
c_p	Specific heat capacity, J kg^{-1} K^{-1}
T	Temperature, K
t	Time, s

It is advantageous that the predominant heat generation takes place mainly in the electrolyte itself, so that the enthalpy change is mainly noticeable here. Responsible for this are the massive movements of the electrolyte due to gas bubbles and magnetic field, as well as the very good thermal conductivity of aluminum (k = 100 W/mK) and electrolyte (k = 0.8 W/mK) [7]. The changed heat generation at anode and cathode contributes to this by the direct contact to electrolyte and aluminum. Thus, the enthalpy change of the liquid electrolyte is equivalent to the enthalpy change of the pot [8].

$$m_{bath}c_{p,bath}\frac{dT_{bath}}{dt} = m_{pot}c_{p,pot}\frac{dT_{pot}}{dt} \tag{2}$$

This approach is only valid until the adjacent areas respond to the heat loss change. Above all, the anodes and the edge crust, over which the majority of the heat is lost and which are the fastest to respond to the change. Due to its very good insulation, the heat loss across the bottom

and the cathode collector bars should be assumed to be constant (15 % TRIMET Cell). The heat loss across the sides can be considered as a simple heat transfer through a wall:

$$\dot{Q}_{L,wall} = hA(T_{bath} - T_{liq}) \tag{3}$$

where:

$\dot{Q}_{L,wall}$ Heat loss rate, W
h Heat transfer coefficient, W m^{-2} K^{-1}
A Area, m²

If the change of heat loss through the sidewall is represented as a fraction τ of the total heat loss, then the remaining heat to be lost is:

$$\dot{Q}_{L,wall} = (1 - \tau)hA(T_{bath} - T_{liq}) \tag{3a}$$

The time it takes for a changed heat loss through the sidewall to influence the heat transfer can be determined as follows [9]:

$$t_L = \frac{4}{\pi^2}\frac{l^2 \rho c_p}{k} ln\frac{4}{\pi\tau} \tag{4}$$

where:

t_L Time till influence on heat loss, s
l Length of the heat flow path, m
ρ, c_p Density and heat capacity of lining material, kg m^{-3}
τ Fractional change of heat loss through the sidewalls
k Thermal conductivity of lining material, W m^{-1} K^{-1}

If the amount of heat through the side walls is reduced by a factor τ = 0.6, the Equation (4) is simplified to:

$$t_L = \frac{3}{\pi^2}\frac{l^2 \rho c_p}{k} \tag{4a}$$

For a 20 cm thick sidewall, a reaction time of about two hours was calculated by [6] with an inaccuracy of one hour. Thus, a calculation of the heat balance with equation (1) will lead to larger deviations after two hours only. A similar behavior can be assumed by changes in the heat transfer of the anode. Already [10] has shown that the temperature of the anode changes visibly when the thickness of the covering material changes. The EPT14 pot has a side wall thickness of about 25 – 30 cm [11], so a new thermal equilibrium should set after about three hours. This can be seen in the experiments (Figure 2). However, the strongly changing heat generation will change the temperature of the cell further on.

2.1. Changes in Bath Chemical Composition

The decrease of liquidus temperature due to the increase in AlF_3 concentration was determined by:

$$\Delta T_{liq} = \frac{dT_{liq}}{d\,(AlF_3)}\Delta(AlF_3) \tag{5}$$

where:

ΔT_{liq} Change in liquidus temperature, °C
AlF_3 Excess AlF_3 concentration, %
$\Delta(AlF_3)$ Change in excess aluminum fluoride concentration in electrolyte.

The values for $dT_{liq}/dAlF3$, derived from the liquidus temperature in [12], are given in Table 1 for a cell with 2.5 % Al_2O_3 and 5.5 % CaF_2. While the CaF_2 content of the pot changes only over a long period of time, the continuous change in the Al_2O_3 content has a direct influence on the liquidus temperature. Within the experiments, it is simply assumed that the alumina control compensates for the Al_2O_3 changes.

Table 1. Rate of change of the liquidus temperature with excess AlF_3.

Excess AlF_3 (mass %)	$\frac{dT_{liq}}{dAlF_3}$ $(\frac{°C}{\%AlF_3})$
4	-0.57
6	-1.56
8	-2.62
10	-3.72
12	-4.86
14	-6.03
16	-7.24
18	-8.48
20	-9.74

3. Electrolyte Temperature, Electrolyte Mass and Electrolyte Chemistry

Due to the influence of the modulation on the temperature, the amount and the chemistry of the electrolyte, four cells were investigated further, especially with regard to the change of the parameters under modulation influence.

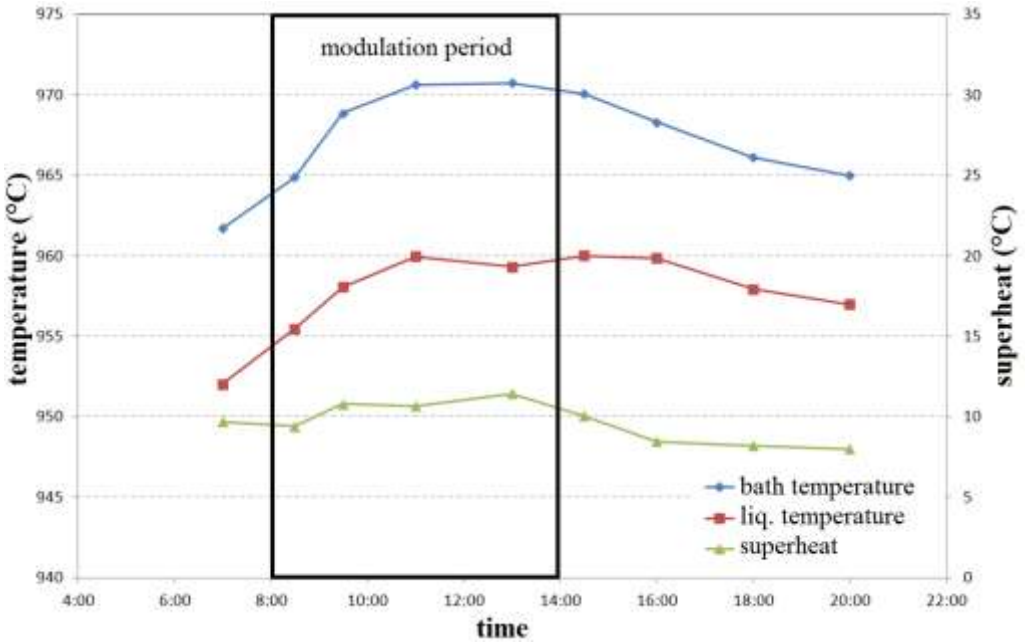

Figure 2. Temperature change at + 12 kA.

As shown in Figure 2 and Figure 3, immediately after raising the current to 180 kA at 8 o'clock, the temperatures increase. While the superheat returns to a normal range at 14 h with the end of modulation, the liquidus and electrolyte temperatures require another 4 – 8 h to cool down. The rapid increase in the liquidus temperature indicates a change in the electrolyte chemistry, which is also reflected in the excess AlF_3 measurements with a 1 % decrease. This chemical change is

due to a loss of the side ledge or cover crust. The fact that the mass of excess AlF_3 decreases shows that this is due to a loss of side ledge, which consists mainly of cryolite [13]. The anode cover crust generally has a higher AlF_3 content [14] due to the absorption of gaseous fluorides from the electrolyte. For this reason, if the cover is lost, the AlF_3 content tends to increase. Although both reactions can occur, the results show that the loss of side ledge is the determining factor (see also Table 2). The phenomenon of melting is largely confirmed by the increase in liquid electrolyte mass. Furthermore, the rate of change from [12] is confirmed. As shown in Table 1 (Chapter 2), the liquidus temperature increases by about 5 ° C, with a 1 % decrease of excess AlF_3 at 12 % of excess AlF_3.

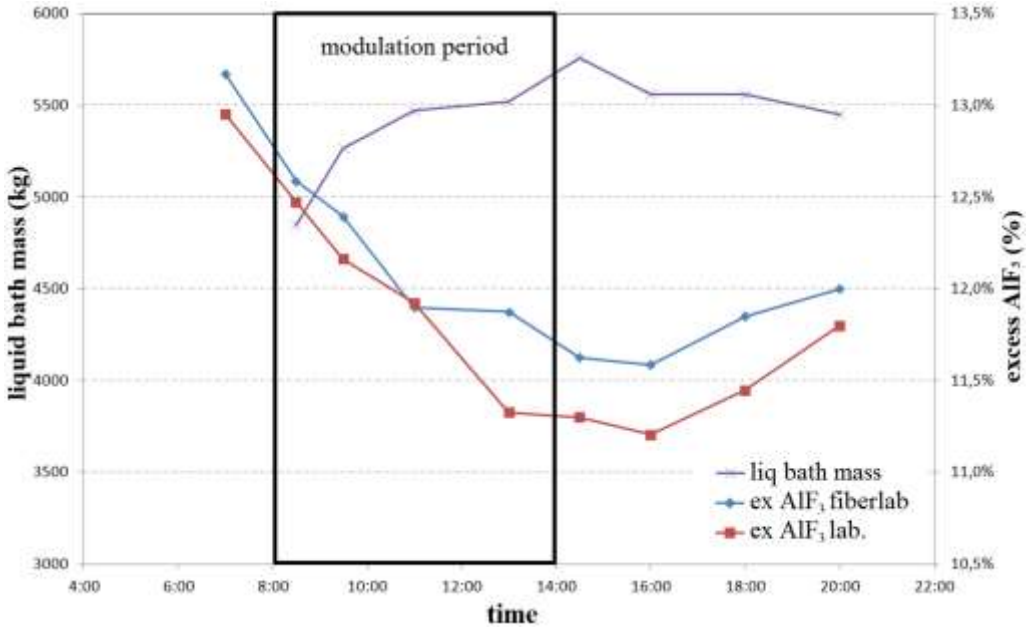

Figure 3. Chemistry change at + 12 kA.

Table 2. Mass % of AlF_3 and composition of solid electrolyte-containing materials in a cell operating at 10 % excess AlF_3 [15].

Material	exAlF_3, %	CaF_2, %	Al_2O_3, %	Na_3AlF_6 ,%	T_{Liq} , °C
Side ledge	0.5 - 6	3 – 5	1 - 3	87 - 95	980 - 990
Bottom sludge	1 - 5	1.6 - 3.5	35 - 60	40 - 60	950 - 964
Cover crust	6 - 12	2 – 4	30 - 50	30 - 48	730 - 950

Table 3. Thermal reactions of a 170 kA electrolytic pot.

Event	Mass (kg)	c_p (J/kg°C)	kWh	Heat distri-bution (%)
Raise bath temperature by 20 °C	4500	1700	42,5	9
Raise liquid Al temperature by 20 °C	10000	900	50	11
Raise anode bottom temperature by 20 °C	5272	1878	55	12
		Latent heat (kJ/kg)		
Melt one ton of side ledge	1000	520	144	31
Melt one ton of lower crust cover	1000	648	180	38

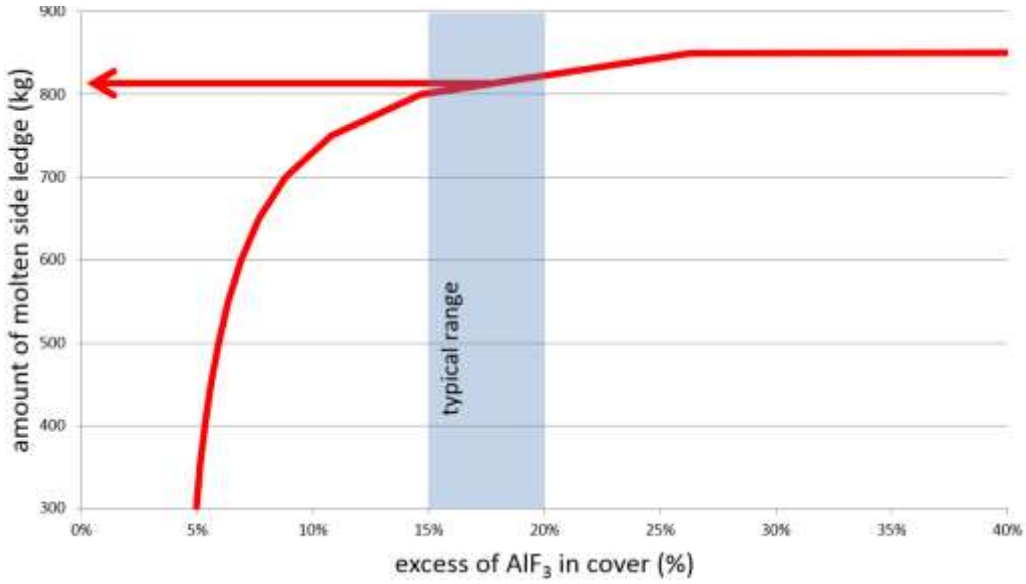

Figure 4. Relation of cover and side ledge loss.

At the start of the modulation during amperage increase to 180 kA, the liquid electrolyte quantity increased by 900 kg on average, while the excess AlF_3 decreased from 12.6 to 11.3 %. The mass fraction of AlF_3 in the lower cover material is approximately 15 – 19 % [14]. The side ledge is pure cryolite or some cases it may have very low excess AlF_3 [13]. Assuming that the side ledge has a surplus of 3 % excess AlF_3, the distribution of molten side ledge to molten cover is calculated to be nine to one (see Figure 4). The amount of heat needed to melt the side ledge and raise the temperature in the cell is given in Table 3Table 3. Thermal reactions of a 170 kA electrolytic pot. The table was supplemented with the ratio of the heat distribution, which results from the measured values (Figure 2), and a heat addition of 212 kWh. It is interesting that in all cells after a short time a temperature plateau is reached, which shows that a new equilibrium has set in. Previous studies [15], [16] have shown that equilibrium without heat exchangers occurs much later. It can be concluded that the reason for the rapid change is the massive cooling reaction by the heat exchangers. With an amperage increase of 18 kA a new operating condition can be achieved after less than 4 h. The significantly lower decrease of the electrolyte and liquidus temperature is due to a slower cooling process. The entire experiment has shown that with the start of the modulation, the cells should be operated with a much higher cooling to get a quicker equilibrium, while after about 3 hours normal cooling can be continued.

3.1. Conclusion

In summary, the results show that regulation of the heat balance with the heat exchanger is possible, but a complete change of the side ledge thickness cannot be avoided. Due to the temperature changes on both sides, inside by the power change and outside by the heat exchangers, the isothermal lines move parallel to each other or away from each other (the temperature change per cm wall thickness increases or decreases). However, the heat exchangers reduce the risk of furnace failure shortly after the power changes and help achieving a steady state in a timely manner.

4. Energy Counter

The previous chapter showed that a new equilibrium occurs within a modulation period. For example, a cell at 960 °C cell may be considered hot after a low-energy phase and cold after a high-energy phase [17]. For this reason, it is extremely important for process control to know

the history of the energy balance. For this, an "Energy Counter" was developed, which determines heat loss and heat input of the cell.

4.1. Equation Determination

The change in heat balance is divided into five sub-points:

- Heat input (cell voltage and current)
- Heat loss (convection, radiation and conduction)
- Heat absorption for making aluminum
- Heat absorption for phase change of the electrolyte
- Sensible heat content (pot temperature changes and working operations such as anode change).

From this, the following basic equation can be determined.

$$\Delta\dot{Q} = \dot{Q}_E - \dot{Q}_L - \dot{Q}_{Al} - \dot{Q}_{phase} - \dot{Q}_I \quad (6)$$

where:

$\dot{Q}_E$ Heat input, W
$\dot{Q}_L$ Heat loss, W
$\dot{Q}_{Al}$ Heat absorption to make aluminum, W
$\dot{Q}_{phase}$ Heat absorption by bath melting, W
$\dot{Q}_I$ Sensible heat content due to temperature change content, W

4.2. Heat input

The heat input can be determined by the product of cell voltage (V_{cell}) and current (I_{cell}). The cell voltage is measured from cell to cell. For this reason, the external voltage drop (V*ext*) must be subtracted for the calculation. The external voltage drop was recorded at 162 kA and the following equation was established:

$$\dot{Q}_E = I_{cell}\left(UV_{cell} - V_{ext}\frac{I_{cell}}{I_{162\ kA}}\right) \quad (7)$$

where:

I current, A
V voltage, V

4.3. Heat loss

To determine the heat loss, more than 50 thermocouples and heat flux sensors were installed at several pots and the readings were used in the following equations:

$$\dot{Q}_{L,convection} = h_c A(T_S - T_0) \text{ [18]} \quad (8)$$
$$\dot{Q}_{L,radiation} = \varepsilon\sigma A({T_S}^4 - T_0^4) \text{ [19]} \quad (9)$$

which can be represented also with the same equation as convection, using an equivalent radiation heat transfer coefficient

$$\dot{Q}_{L,radiation} = h_r A(T_S - T_0) \quad (9a)$$

The conduction heat loss is axially from the collector bars and anode rods.

$$\dot{Q}_{L,conduction} = kA_{cond}\frac{(T_2 - T_1)}{d} \text{ [20]} \quad (10)$$

where:

h_c Heat transfer coefficient, W/m^{2}K^1
T_S Surface temperature, °C
T_0 Ambient temperature, °C
A Area of the heat loss surface, m^2
ε Emissivity, σ = Stefan-Boltzmann constant, W/m^{2}K^4
h_r Equivalent radiation heat transfer coefficient, W/m^{2}K^1
k Thermal conductivity, W/mK
A_{cond} Cross-section of the conductor, m^2
T_2 Conductor temperature at point 2, °C
T_1 Conductor temperature at point 1, °C
d Distance between point 2 and point 1, m

In heat transfer from solid to gas phase, the conductive heat transfer (Equation 10) is absent. The radiation heat loss (Equation 9) is comparable to natural convection heat loss at low surface temperatures and is dominant at high surface temperatures (> 200 °C). As an example, for a steel (emissivity = 0.85) surface temperature of 110 °C and an ambient temperature of 15 °C, the surface heat flux for radiation is 702 W/m² and for natural (h_c = 6,5 W/m^2 K^1) convection 618 W/m². Forced convection heat loss by blowing parallel to the surface at 10 – 30 m/s is 1435 – 3686 W/m². Forced convection by perpendicular flow is more effective as shown by heat transfer coefficients in Table 4. With strong blowing the heat loss could be 27 550 W/m² (heat transfer coefficient of 290 W/m²K in Table 4).

As a basis for the calculation, the outside wall temperatures are measured with thermocouples. These are attached to the bottom, front and long sides of the cell and also above the cell at the superstructure. For the sake of simplicity, all surfaces are treated as smooth surfaces and, depending on the position of the surface, values are chosen for the heat transfer coefficient between 10 and 24 W/m²K [21]. The different values are due to the different air conditions at the cell bottom, side and the hoods.

Table 4. Forced convection heat transfer coefficients [22]

Air movement	Intensity	h_c [W/m²K]
Perpendicular to the metal wall	Light	3.5 - 35
Perpendicular to the metal wall	Moderate	23 - 70
Perpendicular to the metal wall	Strong	58 - 290

For the heat conduction via the cathode collector bars and anode rods, a dynamic value of 6 % of the heat input was assumed [6], [23].

The heat losses calculated by the above formulas are shown in Table 5. The values are comparable to measured values of a heat flow calorimeter [24].

Table 5. Heat losses at 162 kA, cell in normal operation.

Position	Power (kW)	Distribution (%)	Area	Distribution (%)
Total heat loss	325	100		
Exhaust gas flow	104	32	Top	50
Superstructure	59	18	Top	
Heat exchanger	65	20	Side	42
End	32	10	Side	
Longitudinal side	20	6	Side	
Collector bars	19	6	Side	
Bottom	26	8	Bottom	8

4.4. Heat of Reaction, Bath Phase Change and Sensible Heat

4.4.1. Steady State Heat of Reaction

The heat of reaction for production of aluminum is a function of current efficiency. The current efficiency varies typically between 90 and 95 % and is determined by the long term mass of tapped aluminum. Due to energy balance variations and cell erosion, the volume of the liquid metal is variable and the mass of the metal is known only approximately. Furthermore, the mass of aluminum varies because it is tapped only once every 48 hours. On the average, the heat of reaction to make aluminum is [25]:

$$Q_{Al} = V_{Al} I \tag{11}$$

$$V_{Al} = 0.450 + 3.110 \times 10^{-5} T + [1.4316 - 0.03252(1 - \varepsilon) + 2.255 \times 10^{-4} T]\eta \tag{11a}$$

where:

V_{Al} Voltage equivalent of enthalpy of reaction to make aluminium, V
I Pot current, kA
T Bath temperature, °C
η Current efficiency, fraction
ε Fraction of α-alumina in alumina.

4.4.2. Transient: Bath Phase Change

For the melting of the crust no direct measuring device could be installed. An approximate mass of liquid electrolyte can be determined from bath chemical composition. How much energy is required for different thermal changes in the electrolysis cell, is shown in Table 3. Due to the fact that the chemical composition is determined only every 48 hours and with the simplification that melting and solidification in this period remain in balance, this change in energy was neglected in the scheme for the time being. In a second approach, based on the results from Chapter 3 and the basics in Chapter 2, the following equation was integrated into the heat balance.

$$\dot{\boldsymbol{Q}}_{\boldsymbol{phase}} = \boldsymbol{\Delta AlF_3} \times \mathbf{90} \frac{\boldsymbol{kW}}{\boldsymbol{\%AlF_3}} \tag{12}$$

where:

ΔAlF_3 Change of excess AlF_3

4.4.3. Transient: Sensible Heat Content (Enthalpy)

Changes to the cell usually cause a change in temperature and thus change of the enthalpy of the cell. The three biggest influences are the heating / cooling of the cell, an anode change and the addition of alumina and AlF3. While AlF3, alumina and anodes need to be brought up to process temperature and are integrated into the voltage for making aluminum, changing the cell temperature can be either energy loss or gain. The formula used for this is shown below:

$$\dot{Q}_{I,Enthalpy} = \Delta T \times 6.5 \frac{kW}{K} \tag{13}$$

where:

ΔT Change of bath temperature, °C

4.5. Conclusion on Energy Counter

The energy counter can be used to display the current status (Figure 5) as well as the heat quantity difference (Figure 6). If the energy input and the loss are not congruent, the heat loss can be changed by adjusting the volume flow of the heat exchanger via the frequency inverters. Figure 5 shows that the heat input (blue) is lower than the heat loss (green). By lowering the cooling capacity through the heat exchangers (dark green) heat input and loss can be rebalanced.

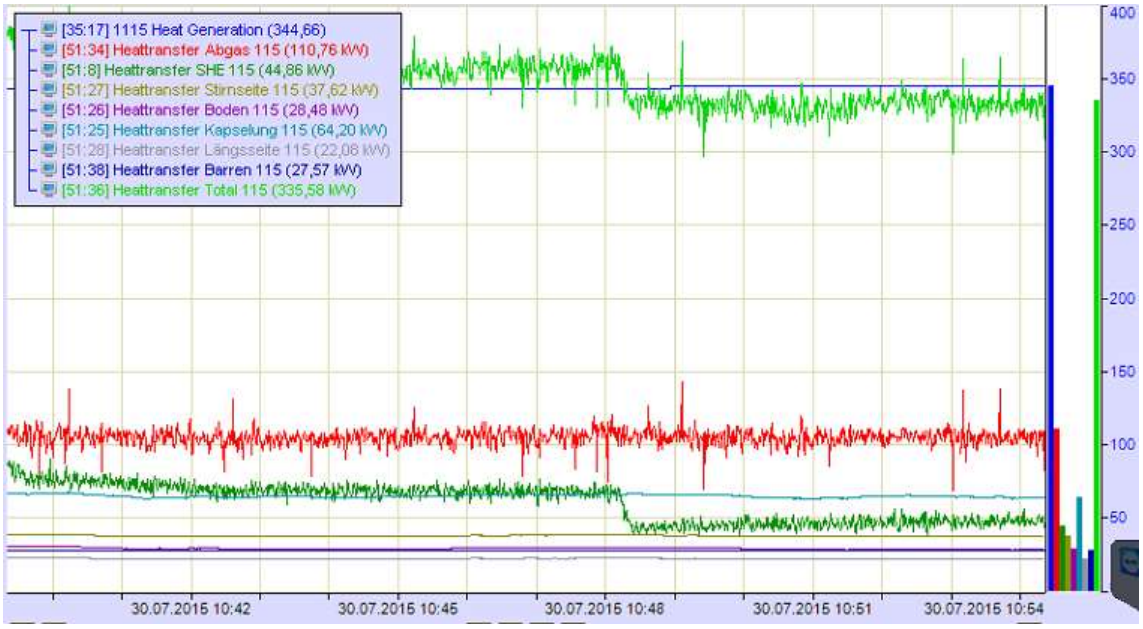

Figure 5. Heat losses in the data acquisition system.

Figure 6. Heat difference over 48 h (blue = heat plus in cell 1114, red = heat plus in cell 1115).

The continuous recording of the heat losses of an electrolysis cell is a novelty and the first step to a concept for a controllable heat loss of an aluminum electrolysis cell. The integration into the process system as well as the extension of the current process system with regard to the chemical changes and possible different process equilibria (Section 3) are described in Section 5.

5. Real-Time Energy Balance Control

Since the invention of the Hall-Héroult process in 1886, an absolutely constant energy supply is the most important guarantee for a stable and energy-efficient production process. Thus, since then, the control concepts are designed for a consistent energy balance. The two control variables for the current system are the bath temperature and the liquidus temperature or bath chemistry. They are controlled by the two control variables: cell voltage and AlF_3 additions. Together with the energy counter, another variable was introduced into the control system - the heat balance.

- Controlled variable thermal state: temperature of the electrolyte
- Controlled variable chemical state: solidification temperature of the electrolyte or excess AlF3
- Controlled heat balance: ΔQ from the Energy counter.

5.1. Approach

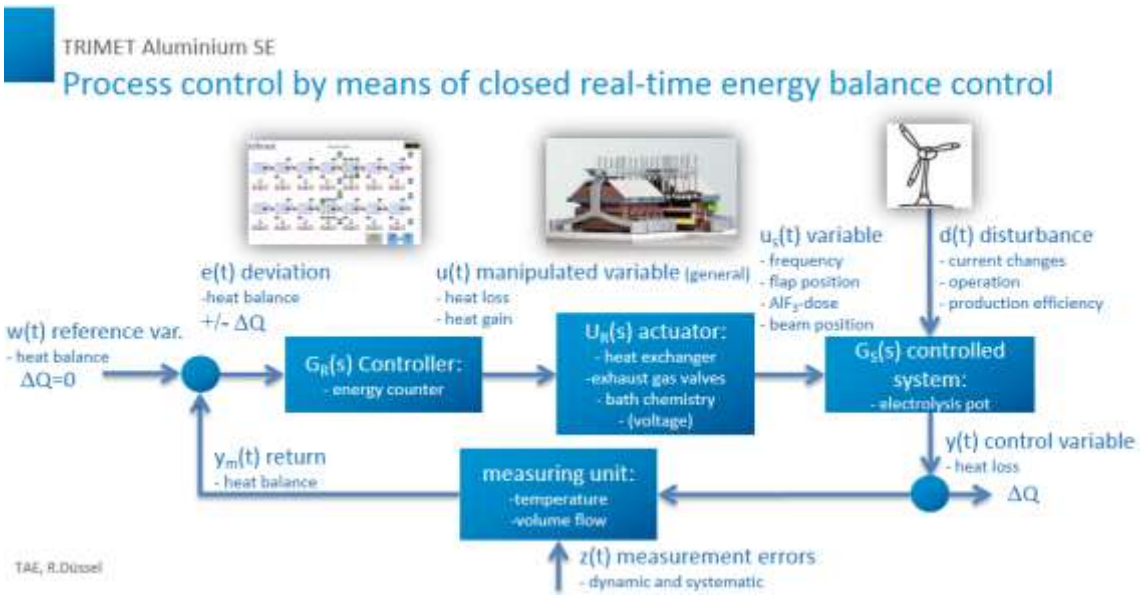

Figure 7. Approach control loop (Patent by TRIMET) [5].

The solution approach is the energy counter itself. Emerging disturbances such as noise and also the old control system itself can be minimized or eliminated. Various control experiments were tested virtually and on the real system with proportional controller (proportionality of current intensity to cooling power) and PI controller. However, due to the complexity of the system, the large number of heat exchangers (528 pieces) to be controlled with only one fan, and the fact that the existing process control system (9-Box) cannot currently be replaced, it has been found that an approximately linear control of the heat balance is the most appropriate.

5.2. Cooling by Heat Balance Difference (PI)

For the control of the cooling, a P and an I component were developed together with the Department of Automation [26]. To realize ΔQ = 0, the energy counter determines a manipulated variable (frequency in Hz) calculated for the fans of the heat exchangers.

$$\Delta\dot{Q} = \dot{Q}_E - \dot{Q}_{L,SHE} - \dot{Q}_{L,rest} - \dot{Q}_{Al} - \dot{Q}_{phase} - \dot{Q}_I = 0$$

$$\dot{Q}_{L,SHE} = \dot{Q}_E - \dot{Q}_{L,rest} - \dot{Q}_{Al} - \dot{Q}_{phase} - \dot{Q}_I$$

$$\dot{V} = \frac{\dot{Q}_{L,SHE}}{\Delta T \times C_p \times \rho \times A \times \frac{3}{2}}$$

$$f = \frac{\dot{V} - 0.3\,\frac{m^3}{s}}{0.26\,m^3} \qquad (14)$$

where:

f Frequency, Hz

$\dot{V}$ Flow rate, $m^3\ s^{-1}$

The I component is calculated using the heat energy difference, Figure 8. If the difference exceeds a fixed positive or negative limit, the frequency is changed by +/- 3Hz.

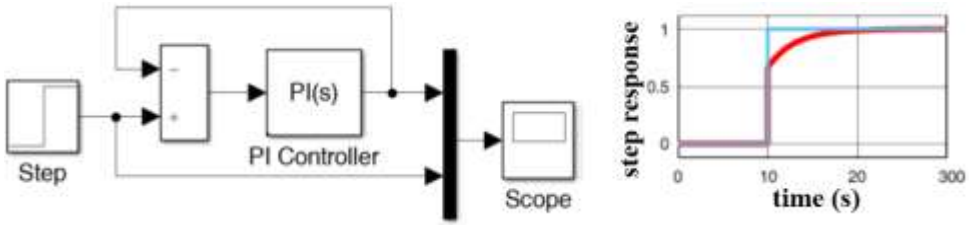

Figure 8. Simplified representation of the PI controller using Shell Heat Exchanger (SHE) and energy counter.

5.2.1. Conclusion

The I component was installed in order to continuously minimize any system deviation occurring. Unfortunately, the previously expressed concerns that the heat balance control and the control concept of the cell (9Box) stimulate each other were confirmed in the test phase. The 9Box system is already parallel working to the alumina control in a multi-size system. By integrating this further control system, its reference variables become interference variables of the existing systems and make the overall system unstable. Furthermore, it is much more effective to counteract the cause of the heat change directly where it develops. The heat is generated mainly in the area of the anode-cathode distance (ACD), thus, a reduction of the ACD during amperage increase and an increase of the ACD during amperage reductions make sense. Finally, with the large number of cells, 120 units with 5280 heat exchangers in one control loop, it is difficult to control with a mean value. Should individual groups heat up and others cool down, then the average over all cells may be within the target range, or if that is not the case, the controller will move some cells out of the range while others will be brought into the range. For the reasons mentioned, a linear control with a simple P element is presented below. By adapting the ACD, the desired result can be achieved in combination with the heat exchangers and the energy counter. On top of that, the proven 9Box control system is used to control individual groups. A combination of both is being developed at the moment in a totally new process control system.

5.3. Proportional Voltage Adjustment

The greatest lever for maintaining the heat balance is adjusting the heat balance by changing the voltage. However, this is only possible to a limited extent because the limits are the minimum cell resistance and an energy-efficient process. Figure 9 shows schematically the process window. The minimum cell resistance with magnetic field compensation is 12.9 μΩ. It is calculated from the minimum cell voltage of 3.85 V (at 162 kA, Figure 10).

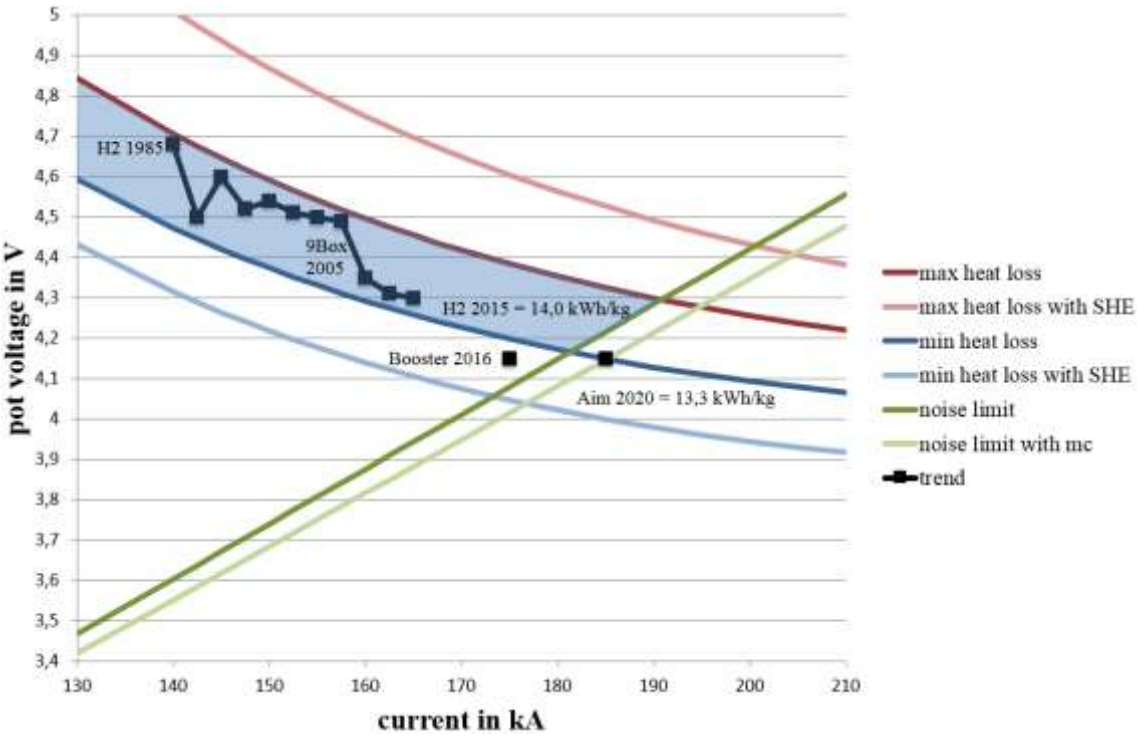

Figure 9. Process window of the EPT14 cell.

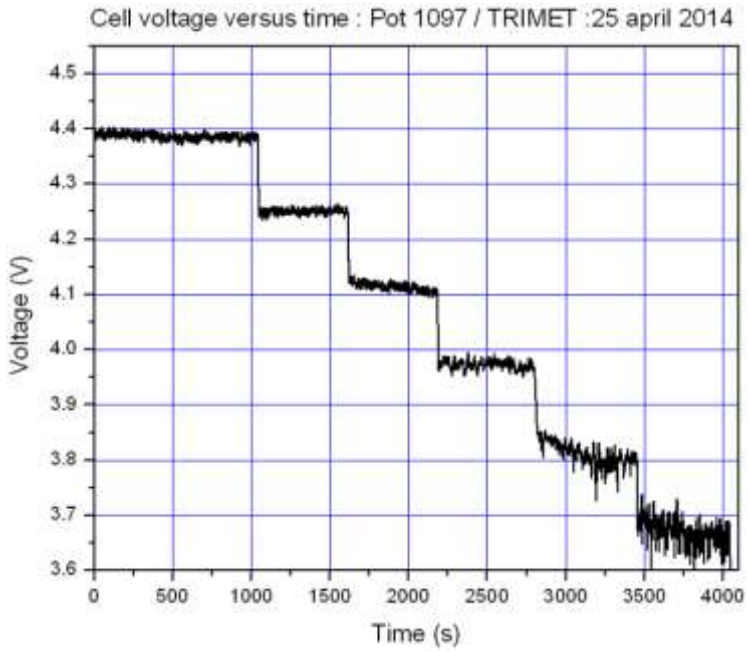

Figure 10. ACD reduction in Cell 1097 without magnetic compensation.

The control of voltage adjustment and heat exchanger control is shown in simplified form in Figure 11Figure 11, where the difference in heat loss between nominal and actual (actual = 302 kW) is shaded. By lowering the cell resistance (green line) to its minimum (green dotted line), the heat loss can be kept approximately constant up to 180 kA (blue line). In addition, with the increase in the cooling capacity of the heat exchanger (red line), the heat loss is kept constant up to about 200 kA (blue dotted line). Above 200 kA, the cell will definitely heat up (red area). Thus, values above 200 kA can only be approached for a short time if no other option for reducing heat, such as raising the exhaust gas flow, is installed.

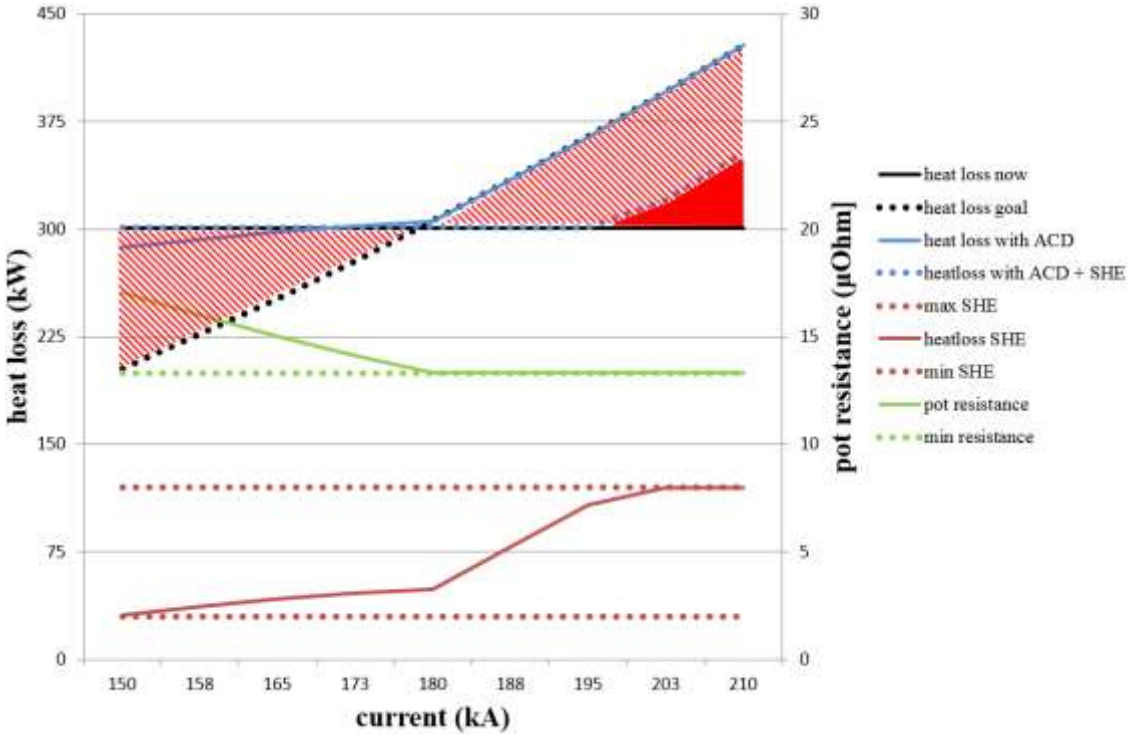

Figure 11: Heat loss control using heat exchangers and ACD changes

5.4. Adjustment of the 9Box

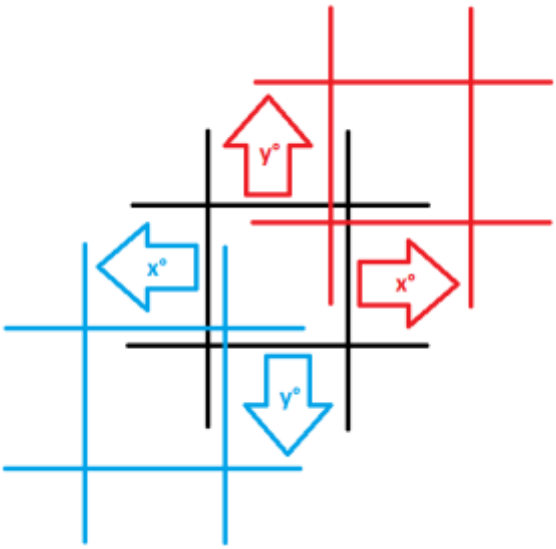

Figure 12. Offset of the 9Box during modulation.

As already described in Section 3, extensive modulation results in a shift of the chemical and thermal equilibrium. If temperature measurements take place during this time, these values produce a manipulated variable change, which in turn itself causes a control difference for the period after the modulation. In addition, heating or cooling causes a further superimposed temperature offset. An offset for the temperature and the liquidus temperature is determined and included into the control, so that the 9-Box control continues to function stable. This disturbance variable connection to the controlled variable is schematically shown in Figure 12.

5.5. Temperature Offset

The ΔQ calculated with the energy counter over a period of 12 h, determines the size of the temperature offset. The limit of ± 8 °C is a quantity investigated by the experiments described in Section 3, which on the one hand represents the maximum loss of SH, and on the other hand guarantees that the system is not changed to a size where it becomes unstable. A more complex calculation has also been made for the chemical part or the liquidus temperature.

$$x' = \frac{1}{40}\frac{^{\circ}C}{kWh} \times \int_{t=-12h}^{0h} \Delta Q dt$$

$$x_{9box\ offset} \begin{cases} -8\ ^{\circ}C & for\ x' \leq -8\ ^{\circ}C \\ 8\ ^{\circ}C & for\ x' \geq 8\ ^{\circ}C \\ & else\ x' \end{cases} \quad (15)$$

where:
x' temperature offset, °C

5.6. The New Algorithm

Finally, the 9Box algorithm is not changed in this step. However, disturbances such as noise are eliminated and occurring calculable (systematic) measurement errors are converted. The energy counter plays an important role in determining the energy balance or the current state of the cell. In order to ensure the process, the concept of minimizing the impact on the system continues to be pursued. The term stability takes on a new meaning. A constant electrolyte temperature is no longer exclusively a guarantee of stability, but an electrolyte temperature that is within a certain temperature range.

The control is described by means of a PT1 element. To compensate for the time offset of the thermal behavior of the side ledge (see Section 2), the PT1 element is shown negatively, so that the step response exceeds the target value and approaches from the opposite side. In Figure 13, the simplified flowchart and its step response are shown schematically. This control behavior is solely for heat loss via the SHE, while the control is done by ACD with a simple P-element with delay.

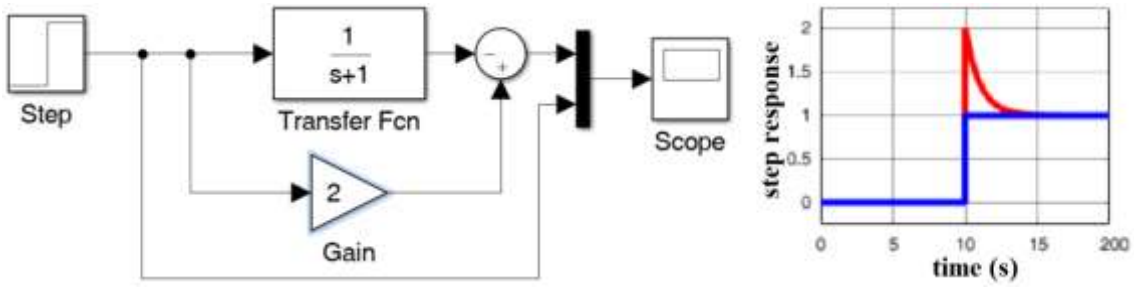

Figure 13. Overshoot of the cooling for faster heat loss adjustment.

Transfer function ACD part:

$$G_{\{ACD\}}(s) = K_{ACD} \tag{16}$$

where:
$G_{\{ACD\}}(s)$ Transfer function
K_{ACD} Proportional amplification

Transfer function heat exchanger part:

$$G_{\{SHE\}}(s) = \frac{-K_{SHE}}{Ts+1} + 2 \tag{17}$$

where:
T reset time, s

The step response of the present PT1 system can be described as follows:

$$y(t) = e^{\frac{-t}{T}+1} \tag{18}$$

where:
$e^{\frac{t}{T}}$ Error value

To compensate for the reaction time of approx. 2 h (Section 2), the heat loss is changed more strongly over a defined period of time. The heat loss change is doubled first and then asymptotically approaches the calculated value. The time constant should be chosen so that the area of the elapsed time (lost heat loss) is equal to the intentionally overcompensated time. Equation (19) shows the calculation and Figure 14 the two areas. For the compensation, a value of T = 7200 s is set for the time constant.

$$\begin{aligned} \int_{7200s}^{\infty} 1 + e^{-\frac{t}{T}} dt &= \int_{0s}^{\infty} 1 dt \\ \Leftrightarrow \int_{7200s}^{\infty} e^{-\frac{t}{T}} dt &= \int_{0s}^{7200s} 1 dt \\ \Leftrightarrow -T \times e^{-\frac{\infty}{T}} + C - \left(-T \times e^{0s/T} + C\right) &= 7200s - 0s \\ \Leftrightarrow T &= 7200\ s \end{aligned} \tag{19}$$

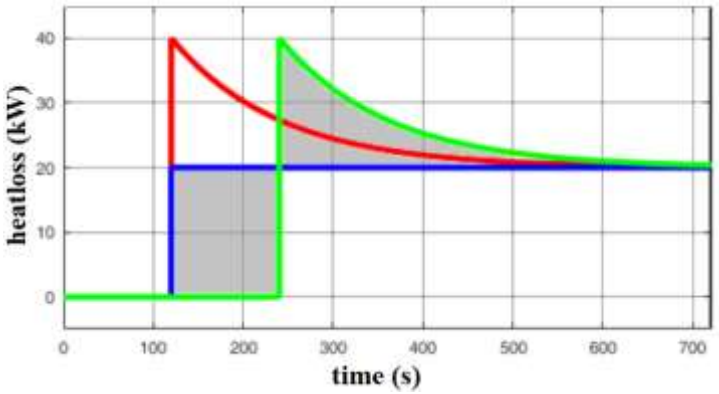

Figure 14. Behavior of the system.

A general virtual system was designed in Matlab and Simulink together with KANNAK [27]. In this system, the 9Box system and the real-time energy balance control with the mentioned control elements were integrated to prove theory before implementing it.

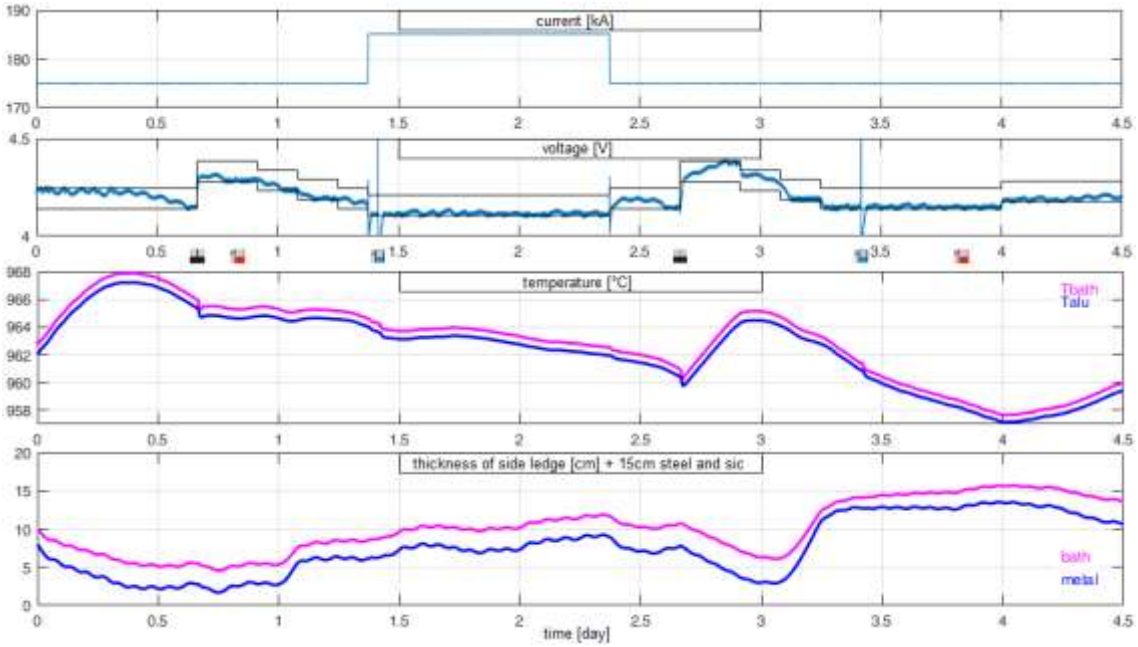

Figure 15. Results from the virtual control system.

The transient calculations showed, that with reduction of the ACD and additional cooling with the heat exchangers it was possible to keep the side ledge (Figure 15). While in a second calculation without cooling and reduction of the voltage, the side ledge was lost quickly (Figure 16). The calculated value of about 3 h cooling reaction time (equation 4a) was confirmed by the model and furthermore verified with thermocouples in tests at the cells. However, a range of 1.5 – 4 h was registered by thermocouples here, which could be related to the wall thickness that was hard to measure accurately.

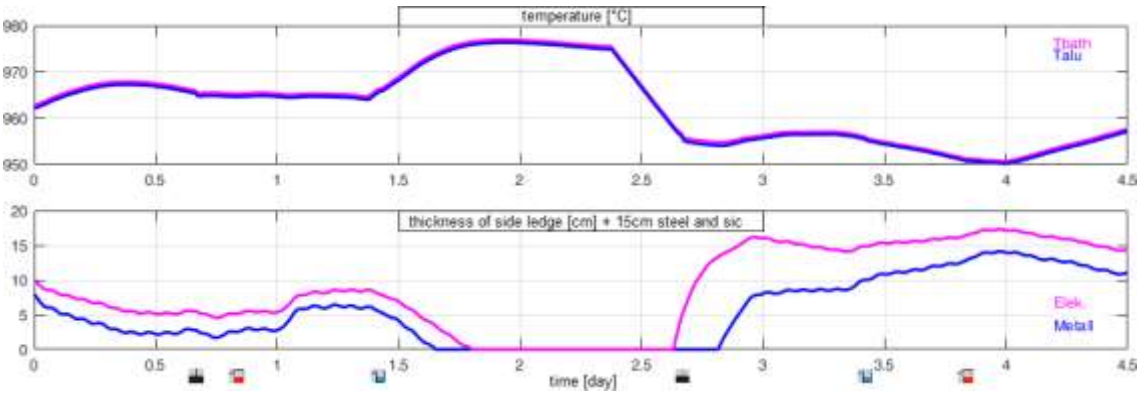

Figure 16. Results from the virtual control system without SHE and ACD adjustment

6. Conclusions

A Megatrend of the next decades is the energy transition from conventional power to renewable. This huge task for our society is comparable to the first moon expedition. It can be a despair challenge for our industry or a winning opportunity. If we want to capture the opportunity, we need a revolution of the aluminium production process. We gave this revolution a name. “The Virtual Battery”. This concept is a landmark project in the German Energy Transition.

Adapting the aluminium smelting process to a flexible power supply needs the rethinking of a number of aspects in the smelting process. Manipulating thermal and magnetic impacts

associated with alternations of amperages are just a few of these aspects. The core element of our Virtual Battery is our new developed control system. Conventional pot control systems are designed for conventional operations and static process targets. This becomes obsolete or even contradictory when operating with power modulation. Hence we need a different approach.

The approach that is outlined here is divided into three areas. The first step is to reduce the energy input as far as possible and to compensate in a subsequent step the heat loss by heat exchangers. Each cell is subject to thermal and process engineering limits, which were intended for the cell at TRIMET Essen. If the minimum cell resistance and the min/max limits of the heat losses are well known, the regulation of the heat balance can be done by changing the resistance. According to Ohm's law the resistance can be adjusted to its minimum inversely proportional to the current. By reaching the resistance minimum the heat loss through the heat exchanger is increased in proportion to further current increases. However, a change in heat loss via the heat exchangers does not occur immediately, but is subject to a reaction time, which was presented in Section 2 and in Section 3. By means of a specifically overcompensating PT1 element, the lagging heat loss change is counteracted, so that a new thermal equilibrium is set up more quickly.

Finally, control system of an existing process control must be adjusted so that it does not counteract the energy flexibility, but promote it. The limits and values, like temperatures and their deviations, of an operating cell have to be modified and the meaning of a stable cell rethought.

7. Prospect

The previous, but also further approaches to the volatile energy input and output show that the flexibilization is associated with loss of efficiency. To minimize this and increase the equivalent storage efficiency of the virtual battery, much more data has to be collected, analyzed and processed than in the case of the current process. For this purpose, appropriate measurement and data transmission techniques are to be developed, as well as further flexibility measures for the cell. The control of the heat loss through the side walls comprises only about 20 – 30 % of the heat loss of an electrolytic cell. To increase the efficiency, the exhaust gas flow over the top can be considered in the next step. The changes mentioned must be sensibly integrated into the existing control and monitoring systems. A high degree of automation is required here in order to analyze and meaningfully use the resulting data volumes. In particular, long-term effects, such as the impact on the age of an electrolysis cell, have not yet been explored. The question to be answered is to what extent the flexibilization involves shortening the service life and how this reduction in service life can be counteracted by suitable measures and materials.

So far, the main focus has been on the recording of heat balances, temperatures and voltages. In the age of BigData, it would be possible to more accurately record input controls on alumina and aluminum fluoride levels to account for the chemical equilibrium. Furthermore, with the aid of (mass) data-based recording, monitoring and control of as many relevant process parameters as possible, the operation of an aluminum electrolysis under conditions of flexibilization with regard to wear and energy consumption could be improved. These data have been collected for years, but some have neither been evaluated nor stored nor used for regulation or simple control. To reduce the complexity, the influence of the interacting processes, which should also be included in a novel process regulation, has not been taken into account. Finally, in a novel process control, the energy counter, the real-time energy balance control and the cell control can be interconnected in a multi-size system. This way, the behavior of the cell can be predicted with the help of the virtual system and react to it at an early stage. This very extensive project must include all three levels, from the measurement acquisition (hardware), through the control

(hardware + software), to visualization (software). The foundation for this project has been laid and TRIMET is ready to embark on this paradigm shift in aluminum production.

8. References

1. L.J. Pinheiro Leal Nunes, A. Vianna da Silva, and G. Soutinho, Power modulation on Valesul P-19 pots, *Light Metals* 1998, 1267–1271
2. A.C. Brant Filho, A.A.B. Queiroz, E. Macedo, J.E. Pena, and M.A. Mol Santos, The operation of a smelter with power modulation, *Light Metals* 1992, 357–362.
3. Wolfgang Schmidt-Hatting, Theoretische Zusammenhänge zwischen Ofenstrom und Ofenspannung bei Energiespannen, *Alusuisse Hüttenlaboratorium*, 1974.
4. Wolfgang Schmidt-Hatting, Hans O. Bohner, and T. Tschopp, Anleitung für die Überwindung von Energiespannen, *Alusuisse Zürich*, 1975.
5. Roman Düssel, Entwicklung eines Regelungskonzepts für Aluminium-Elektrolysezellen unter Berücksichtigung einer variablen Stromstärke und eines regelbaren Wärmeverlusts, *Dissertation*, TRIMET Aluminium SE & Bergische Universität Wuppertal, Lehrstuhl für Mess-, Steuerungs-, Regelungstechnik, 2017.
6. M.P. Taylor, W.D. Zhang, V. Wills, and S. Schmid, A dynamic model for the energy balance of an electrolysis cell, *Chemical Engineering Research and Design*, Vol. 74, Issue 8 November 1996, 913-933.
7. Vladimir A. Khokhlov et al., Vladimir A. Khokhlov et al., Thermal conductivity in cryolitic melts - new data and its influence on heat transfer in aluminium cells, *Light Metals* 1998, 501-506.
8. Mark P. Taylor and John J. Chen, Technique for low amperage potline operation for electricity grid storage, *Metallurgical and Materials Transactions E*, March 2015, 87-98.
9. David B. Stewart, Time-domain transient thermal response of structural elements, *Elsevier Ltd. Building and Environment,* Volume 16, Issue 2, 1993, 87–91.
10. Evan W. Andrews, Marc P. Taylor, Greg L. Johnson and Ian Coad, The Impact of Anode Cover Control and Anode Assembly Design on Reduction Cell Performance, *Light Metals* 2005, 357–362.
11. Thomas Pursche, Messdatenerfassung und Korrelationsauswertung von Temperaturen und Wandstärken in Aluminiumöfen, *Masterthesis*, TRIMET Aluminium SE & Bergische Universität Wuppertal, Lehrstuhl für Automatisierungstechnik / Informatik, 2014.
12. Asbjørn Solheim et al., Liquidus temperature and alumina solubility in the system Na_3AlF_6 - AlF_3 – LiF – CaF_2 – MgF_2, *Light Metals* 1995, 451-460.
13. Asbjørn Solheim and Lisbet I.R. Stoen, On the composition of solid deposits frozen out of cryolite melts, *Light Metals* 1997, 325-332.
14. Qinsong Zhang, Mark Taylor, John Chen, David Cotton, Tania Groutzo, and Xiaodong Yang, Composition and thermal analysis of crust formed from industrial anode cover, *Light Metals* 2013, 675-680.
15. M.A. Stam and J. F. Schaafsma, the impact of power modulation on the cell dynamics, *Proceedings of Ninth Australasian Aluminium Smelting Conference and Workshops*, Terrigal, Australia, 4 – 9 November 2007.
16. David Eisma and Pretesh Patel, Challenges of Power Modulation, *Light Metals* 2009, 327-332.
17. Till C. Reek, Power Modulation of Aluminium Reduction Cells - Operational Constraints and Process Limits, *PhD thesis*, 2015, The University of New South Wales, Sydney, Australia.
18. I. Kretzschmar, H.-J. und Kraft, Kleine Formelsammlung Technische Thermodynamik, *4. Auflage. Fachbuchverlag Leipzig im Carl Hanser Verlag München*, 2011.

19. K.-H. Grote and J. Feldhusen, Taschenbuch für den Maschinenbau. *Springer Verlag*, 2014.
20. Jean Baptiste Joseph Fourier, Théorie analytique de la chaleur, *Mémoires de l'Academie royal des Sciences de l'Institut de France,* 1822, Paris.
21. Pascal Lavoie, Sankar Namboothiri, Mark Dorreen, John JJ Chen, Donald P Zeigler, and Mark P Taylor, Increasing the power modulation window of aluminium smelter pots with shell heat exchanger technology, *Light Metals* 2011, 369-374.
22. Günter Cerbe and Hans-Joachim Hoffmann, *Einführung in die Wärmelehre*, 1987
23. Jay N. Bruggeman, Pot Heat Balance Fundamentals, *6th Australasian Aluminium Smelting Conference and Workshop,* Queenstown, New Zealand 22 – 27 November 1998, 167-190.
24. Sercan Koyuncuoglu, Analytische und messtechnische Wärmebilanz an einer Elektrolysezelle, *Bachelorthesis*, 2014, TRIMET Aluminium SE & Bergische Universität Wuppertal, Lehrstuhl für Mess-, Steuerungs-, Regelungstechnik.
25. Abdalla Al Zarouni et al., Energy and mass balance of DX+ reduction cells, *31st International Conference of ICSOBA and 19th Conference Aluminium Siberia,* Krasnoyarsk, Russia, 4 – 6 September, 2013, *TRAVAUX* 42, 494-498.
26. Dietmar Tutsch, Experimentelle Untersuchungen zur Regelung der Kühlung eines Ofens mithilfe von Wärmetauschern, *Abschlussbericht Ziel 2 Projekt, Virtuelle Batterie*, 2016, TRIMET Aluminium SE & Bergische Universität Wuppertal.
27. Jacques Antille, Rene von Kaenel, Louis Bugnion, A Cell Simulator for optimizing operation practices and process control, *33rd International Conference of ICSOBA,* Dubai, UAE, 29 November – 1 December 2015, *TRAVAUX* 44, 635-647.